

# Electronic Correlation Effects on Stabilizing a Perfect Kagome Lattice and Ferromagnetic Fluctuation in $\text{LaRu}_3\text{Si}_2$

Yilin Wang<sup>1</sup>

<sup>1</sup>*Hefei National Laboratory for Physical Sciences at Microscale,  
University of Science and Technology of China, Hefei, Anhui 230026, China*  
(Dated: March 23, 2023)

A perfect Kagome lattice features flat bands that usually lead to strong electronic correlation effects, but how electronic correlation, in turn, stabilizes a perfect Kagome lattice has rarely been explored. Here, we study such effect in a superconducting ( $T_c \sim 7.8$  K) Kagome metal  $\text{LaRu}_3\text{Si}_2$  with a distorted Kagome plane consisting of pure Ru ions, using density functional theory plus  $U$  and plus dynamical mean-field theory. We find that increasing electronic correlation can stabilize a perfect Kagome lattice and induce substantial ferromagnetic fluctuations in  $\text{LaRu}_3\text{Si}_2$ . By comparing the calculated magnetic susceptibilities to experimental data,  $\text{LaRu}_3\text{Si}_2$  is found to be on the verge of becoming a perfect Kagome lattice. It thus shows moderate but non-negligible electronic correlations and ferromagnetic fluctuations, which are crucial to understanding the experimentally observed non-Fermi-liquid behavior and the pretty high superconducting  $T_c$  of  $\text{LaRu}_3\text{Si}_2$ .

Keywords: Electronic Correlation, Kagome lattice,  $\text{LaRu}_3\text{Si}_2$ , Ferromagnetic Fluctuation, Flat bands

## I. INTRODUCTION

A perfect Kagome lattice features flat bands due to the destructive interference of electron hoppings within the geometrically frustrated structure<sup>1-5</sup>. When flat bands are near the Fermi level, it usually induces strong electronic correlation effects such as unconventional superconductivity<sup>6-11</sup>, magnetism<sup>2,3</sup>, topological phases<sup>5</sup> and exotic charge density waves<sup>12,13</sup>. In recent years, these flat-bands-induced correlation effects have been widely studied in Kagome metals, for example,  $\text{FeSn}$ <sup>14,15</sup>,  $\text{FeGe}$ <sup>13,16</sup>,  $\text{Fe}_3\text{Sn}_2$ <sup>17-19</sup>,  $\text{CoSn}$ <sup>20-24</sup>,  $\text{RT}_6\text{Ge}_6$  (R=rare-earth elements, T=Mn, Cr)<sup>25,26</sup>. But how electronic correlation, in turn, stabilizes a perfect Kagome lattice has rarely been explored. Here, we study such effect in a Kagome metal  $\text{LaRu}_3\text{Si}_2$ <sup>27-31</sup>, using density functional theory (DFT) plus  $U$ <sup>32</sup> and plus dynamical mean-field theory (DMFT)<sup>33-35</sup>.

$\text{LaRu}_3\text{Si}_2$  is a superconductor with a highest  $T_c \sim 7.8$  K<sup>27</sup> among the known Kagome superconductors at ambient conditions. It is a paramagnetic metal at high-temperature. Non-Fermi-liquid (NFL) behavior was inferred from transport experiments, indicating substantial electronic correlations from Ru-4d orbitals<sup>29</sup>. A recent DFT calculation based on the electron-phonon coupling mechanism yields a  $T_c \sim 1.2$  K, much smaller than the experimental value<sup>30</sup>, also indicating other factors such as electronic correlations and magnetic fluctuations must be considered to understand its superconductivity.

The perfect Kagome structure of  $\text{LaRu}_3\text{Si}_2$  with space group  $P6/mmm$  is shown in Fig. 1(a) and 1(c). The Kagome layer consists of pure Ru atoms, different from most other Kagome materials in which an anion usually resides in the center of the hexagon of the Kagome structure. Adjacent to the Kagome layer is a layer consisting of a triangular lattice of La and a honeycomb lattice of Si. However, a previous X-Ray diffraction study shows that  $\text{LaRu}_3\text{Si}_2$ , in reality, crystallizes into a slightly distorted

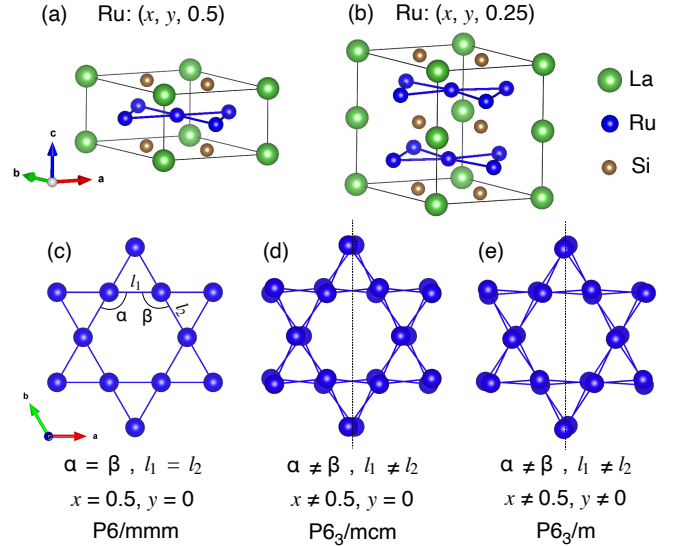


FIG. 1. Three possible crystal structures of  $\text{LaRu}_3\text{Si}_2$  with a Kagome plane consisting of pure Ru atoms. (a),(c) Perfect Kagome structure. (b),(d),(e) Two possible distorted Kagome structures with a doubling of the  $c$ -axis. (c)-(e) Top view of the Kagome planes. The angles  $\alpha, \beta$  and side lengths  $l_1, l_2$  of the hexagon, the fractional coordinates of Ru atoms  $x, y$ , and the space group are shown, respectively. The crystal structures are constructed by VESTA<sup>36</sup>.

Kagome structure with a doubling of the  $c$ -axis and the space group  $P6_3/m$ <sup>27</sup> (see Fig. 1(b) and 1(e)). Given only one kind of ion (Ru) present in the Kagome layer of  $\text{LaRu}_3\text{Si}_2$ , it provides an ideal platform for studying its electronic correlation effects on stabilizing a perfect Ru Kagome lattice, since it rules out possible crystalline field effects of anion on the stability of the Kagome lattice.

Our calculations find that increasing electronic correlation can stabilize a perfect Kagome lattice and induce substantial ferromagnetic fluctuations in  $\text{LaRu}_3\text{Si}_2$ . By

comparing the calculated magnetic susceptibilities to experimental data,  $\text{LaRu}_3\text{Si}_2$  is found to be on the verge of the transition from a distorted to a perfect Kagome lattice. It thus shows moderate but non-negligible electronic correlations and ferromagnetic fluctuations, consistent with the experimentally observed NFL behavior<sup>29</sup>. Furthermore, our calculations show that the distorted Kagome structure of  $\text{LaRu}_3\text{Si}_2$  may hold higher symmetry (space group  $P6_3/mcm$ , see Fig. 1(d)) than that reported by previous experiment ( $P6_3/m$ )<sup>27</sup>, which should be further examined by high-resolution crystal structure refinement with high-quality samples.

## II. METHODS

We perform DFT+ $U$  calculations using the VASP package<sup>37,38</sup>, with exchange-correlation functional of both local density approximation (LDA) and generalized gradient approximation (GGA)<sup>39</sup>. The energy cutoff of the plane-wave basis is set to be 500 eV, and a  $\Gamma$ -centered  $21 \times 21 \times 21$  K-point grid is used. The internal atomic positions are relaxed in the non-magnetic states, until the force of each atom is smaller than 1 meV/Å. The rotationally invariant DFT+ $U$  method introduced by Liechtenstein *et al.*<sup>40</sup> is used, which is parameterized by Hubbard  $U$  and Hund's coupling  $J_H$  (LDAUTYPE=1 or 4). It turns out that the spin-orbital coupling (SOC) of Ru would not change the main conclusions, so we only present the non-SOC results in the main text, and a SOC result is presented in the Supporting Information (Fig. S1)<sup>41</sup>. The energies of two magnetic orders, ferromagnetic (FM) and A-type anti-ferromagnetic (AFM) (Fig. S2)<sup>41</sup>, are also calculated by GGA+ $U$ .

We also perform fully charge self-consistent LDA+DMFT calculations in the paramagnetic states of  $\text{LaRu}_3\text{Si}_2$ , using the code EDMFTF developed by Haule *et al.*<sup>42,43</sup> based on the WIEN2K package<sup>44</sup>. We choose a wide hybridization energy window from -10 to 10 eV with respect to the Fermi level. All five Ru-4d orbitals are considered as correlated ones and a local Coulomb interaction Hamiltonian with rotationally invariant form is applied. The local Anderson impurity model is solved by the continuous time quantum Monte Carlo (CTQMC) solver<sup>45</sup>. We use an "exact" double counting scheme invented by Haule<sup>46</sup>. The self-energy on real frequency  $\Sigma(\omega)$  is obtained by the analytical continuation method of maximum entropy. We follow the method introduced by Haule *et al.*<sup>47</sup> to perform structure relaxation in the framework of LDA+DMFT. All the calculations are performed at  $T = 290$  K. Following Ref.<sup>43</sup>, we use the Yukawa representation of the screened Coulomb interaction, in which there is a unique relationship between  $U$  and  $J_H$ . If  $U$  is specified,  $J_H$  is uniquely determined by a code in EDMFTF<sup>48</sup>. Their values are tabulated in the Supporting Information (Table S1)<sup>41</sup> and are also used for the DFT+ $U$  calculations.

To reveal the role of electronic correlation effects on

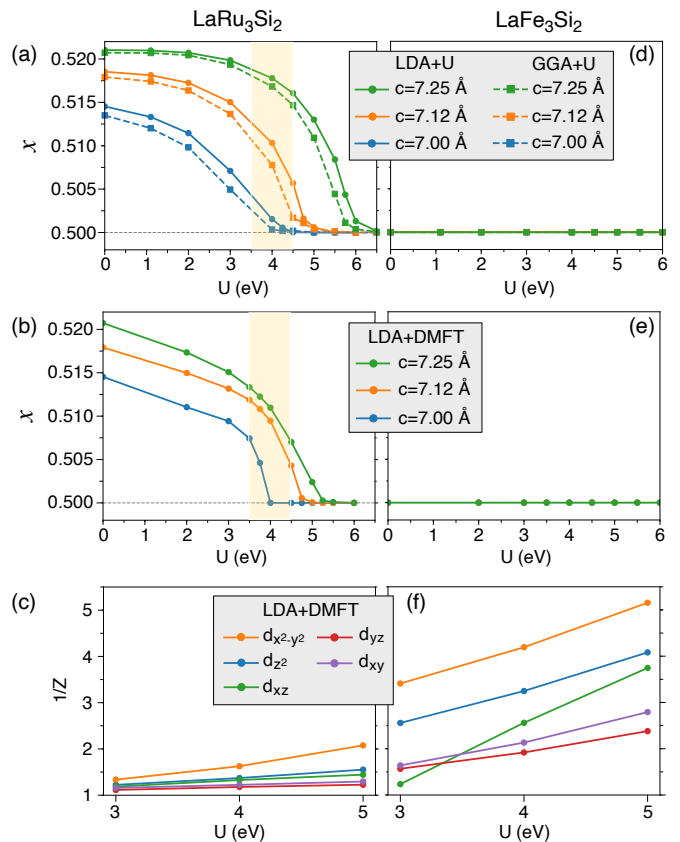


FIG. 2. Electronic correlation effects on stabilizing a perfect Kagome lattice. (a),(d) Fractional coordinates  $x$  of Ru (Fe) relaxed by LDA+ $U$  and GGA+ $U$  as functions of Hubbard  $U$ , for different lattice parameter ratio  $c/a$  with the fixed crystal volume of experiment.  $c = 7.12$  Å is the experimental value.  $x = 0.5$  for a perfect Kagome lattice. (b),(e)  $x$  relaxed by LDA+DMFT as functions of  $U$ . The yellow area mark that  $\text{LaRu}_3\text{Si}_2$  is on the verge of becoming a perfect Kagome lattice. (c),(f) LDA+DMFT calculated mass-enhancement of Ru-4d (Fe-3d) orbitals due to electronic correlations, as functions of  $U$ . (a)-(c) for  $\text{LaRu}_3\text{Si}_2$  and (d)-(f) for  $\text{LaFe}_3\text{Si}_2$ .

stabilizing a perfect Kagome lattice in  $\text{LaRu}_3\text{Si}_2$ , (1) we vary the Hubbard  $U$  from 0 to 6 eV in our calculation; (2) we perform a comparative study on a hypothetical crystal structure  $\text{LaFe}_3\text{Si}_2$  with the same lattice parameters and initial atomic positions as  $\text{LaRu}_3\text{Si}_2$ , since Fe-3d orbitals are expected to show stronger electronic correlations than Ru-4d orbitals. To uncover how the adjacent  $\text{LaSi}_2$  layers affect the stability of the  $\text{Ru}_3$  Kagome layer, we also perform comparative calculations by varying the lattice parameter ratio  $c/a$  with the fixed crystal volume from experiment. The experimental lattice parameters are  $a = 5.676$  Å,  $c = 7.12$  Å, which gives a volume of  $198.65$  Å<sup>3</sup><sup>27</sup>. Crystal structure with space group  $P6_3/m$  and Ru sites at  $(x = 0.52, y = 0.01, z = 0.25)$  is constructed as the starting point for relaxation (see Fig. 1(b) and 1(e)). However, all the relaxations converge to the higher symmetry structure with space group  $P6_3/mcm$

( $x \neq 0.5$ ,  $y = 0$ ,  $z = 0.25$ ), where an additional  $C_2$  and mirror symmetry is present (see Fig. 1(d)). Therefore, we will only discuss the results of space group  $P6_3/mcm$  below.

### III. RESULTS

Fig. 2(a)-(b) and (d)-(e) show the fractional coordinate  $x$  of Ru (Fe) relaxed by LDA+U, GGA+U and LDA+DMFT methods, for different  $c/a$  ratio. For  $\text{LaRu}_3\text{Si}_2$ , as increasing  $U$ , all the methods yield a tendency that  $x$  is decreasing and approaching to the value of a perfect Kagome lattice ( $= 0.5$ ). We note that  $\text{LaFe}_3\text{Si}_2$  converges to the perfect Kagome structure even at  $U = 0$ . Comparing to LDA+U, the GGA+U method that is expected to better describe the correlation effects, gives smaller  $x$  (dashed curves in Fig. 2(a)). Fig. 2(c) and (f) show the LDA+DMFT calculated orbital-resolved quasi-particle mass-enhancement,  $m^*/m^{DMFT} = 1/Z$ , due to the electronic correlation effects, where  $Z$  is quasi-particle weight. The system is more correlated as  $1/Z$  deviates more from 1. The electronic correlation become stronger as increasing  $U$ , and  $\text{LaFe}_3\text{Si}_2$  shows much stronger correlation than  $\text{LaRu}_3\text{Si}_2$  as expected. The most correlated orbital is  $d_{x^2-y^2}$  which contributes to the flat bands near the Fermi level (see below). Therefore, these results indicate that strong electronic correlation would stabilize a perfect Kagome lattice consisting of transition metal ions in the system of  $\text{LaX}_3\text{Si}_2$  ( $X=\text{Ru}, \text{Fe}$ ).

Fig. 2(a)-(b) also show that increasing the lattice parameter ratio  $c/a$ , i.e., longer distance between the  $\text{Ru}_3$  Kagome layer and  $\text{LaSi}_2$  layer, tends to increase  $x$  and distort the Kagome plane. Thus, larger Hubbard  $U$  is required to stabilize a perfect Kagome lattice at larger ratio of  $c/a$ .

Fig. 3(a) and (d) show the local magnetic susceptibilities  $\chi_{\text{loc}}(T)$  calculated by LDA+DMFT for different  $U$ . For  $\text{LaRu}_3\text{Si}_2$ ,  $\chi_{\text{loc}}(T)$  shows Pauli paramagnetism behavior at  $U = 3$  eV, while it shows a Curie-Weiss-like behavior at  $U = 5$  eV. In between,  $\chi_{\text{loc}}(T)$  slightly increases as decreasing temperature, which is consistent with that measured by experiment (see Fig.7 in Ref.<sup>29</sup>). Based on this, we infer that the actual Hubbard  $U$  for  $\text{LaRu}_3\text{Si}_2$  is about 4 eV. At this  $U$  value,  $\text{LaRu}_3\text{Si}_2$  is thus found to be on the verge of crystallizing into a perfect Kagome structure, according to the relaxation results at the experimental lattice parameters shown as the orange curves in Fig. 2(a),(b). At  $U = 4$  eV, the mass-enhancement of the most correlated orbital  $d_{x^2-y^2}$  is about 1.63 (Fig. 2(c)). This indicates a moderate electronic correlation in  $\text{LaRu}_3\text{Si}_2$ , consistent with a slightly large Wilson ratio  $R = 2.88$  ( $R = 1$  for non-interacting electron gas) and a NFL contribution to the electronic specific heat, found by the transport experiment<sup>29</sup>. In contrast,  $\chi_{\text{loc}}(T)$  shows a well-defined Curie-Weiss behavior for  $\text{LaFe}_3\text{Si}_2$ , indicating much stronger electronic

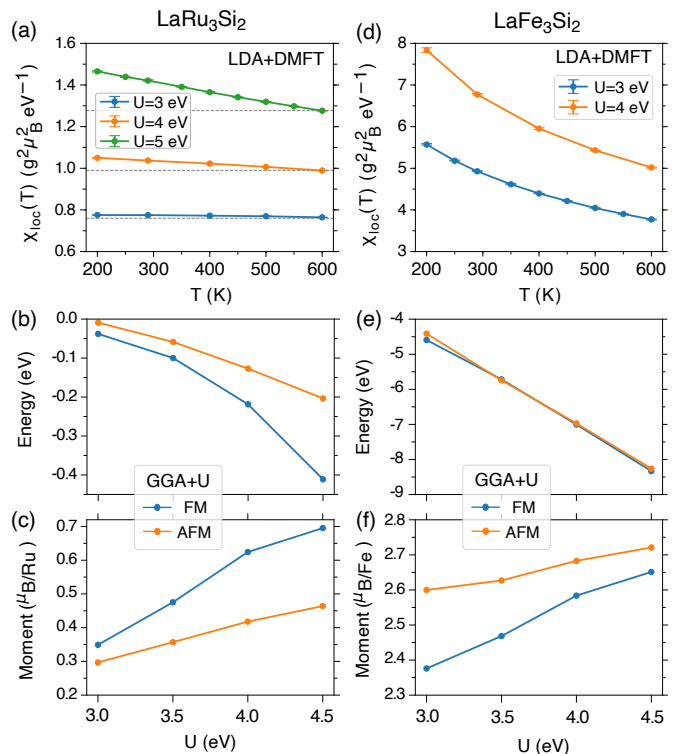


FIG. 3. Electronic correlation induced magnetism. (a),(d) Local magnetic susceptibilities calculated by LDA+DMFT as functions of temperature  $T$  for different  $U$  values. (b),(e) The energies (per unit cell) of FM and AFM orders with respect to the non-magnetic state as functions of  $U$ , calculated by GGA+U. (c),(f) Ordered magnetic moment in the FM and AFM states. (a)-(c) for  $\text{LaRu}_3\text{Si}_2$ , the crystal structures relaxed at the corresponding  $U$  are used. (d)-(f) for  $\text{LaFe}_3\text{Si}_2$ . The experimental lattice parameters,  $a = 5.676\text{\AA}$  and  $c = 7.12\text{\AA}$ , are used for both compounds.

correlation and magnetism.

Fig. 3(b) and (e) show the energies of the FM and AFM orders with respect to the non-magnetic phase calculated by GGA+U, and Fig. 3(c) and (f) show the corresponding ordered magnetic moments.  $\text{LaFe}_3\text{Si}_2$  has very low energies in magnetic states compared to its non-magnetic state and large ordered magnetic moments, suggesting that it tends to order as decreasing temperature. Its FM and AFM states are very close in energies, indicating comparable inter-layer FM and AFM couplings.  $\text{LaRu}_3\text{Si}_2$  shows much weaker magnetism compared to  $\text{LaFe}_3\text{Si}_2$ , but the FM and AFM states are still found to be energetically stable at the static mean-field level. Its FM state has significantly lower energy than the AFM state. Although no magnetic orders have been observed experimentally in  $\text{LaRu}_3\text{Si}_2$ , the stable FM state found by GGA+U calculation suggests that substantial FM fluctuations may exist in  $\text{LaRu}_3\text{Si}_2$ . Such FM fluctuations should be attributed to the flat bands near the Fermi level, derived from the Kagome lattice.

Fig. 4 shows the LDA and LDA+DMFT calculated

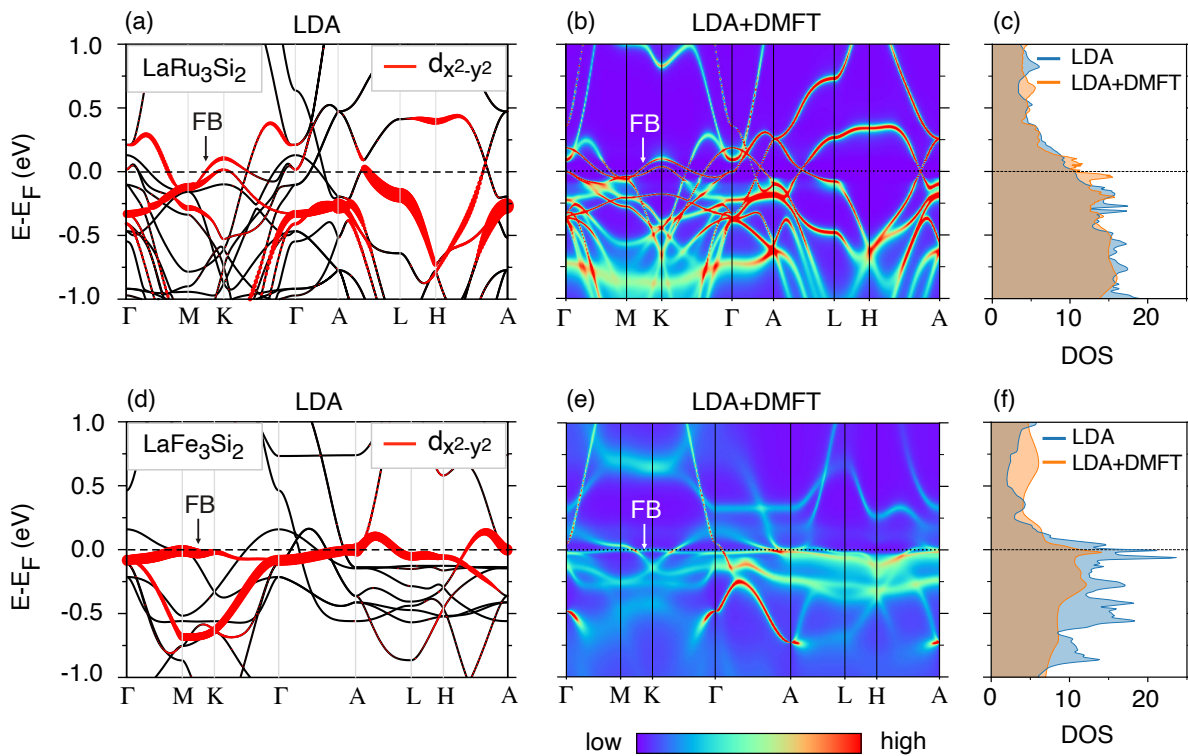


FIG. 4. Flat band near Fermi level. (a),(d) LDA calculated band structures. The flat bands (FB) with  $d_{x^2-y^2}$  character are shown in red. (b),(e) LDA+DMFT calculated spectrum function  $A(k, \omega)$  at  $U = 4$  eV,  $J_H = 0.782$  eV and  $T = 290$  K. (c),(f) The corresponding density of states. (a)-(c) for  $\text{LaRu}_3\text{Si}_2$ , the crystal structure relaxed by LDA+DMFT at  $U = 4$  eV,  $J_H = 0.782$  eV is used. (d)-(f) for  $\text{LaFe}_3\text{Si}_2$ . The experimental lattice parameters,  $a = 5.676\text{\AA}$  and  $c = 7.12\text{\AA}$ , are used for both compounds.

band structures and density of states (DOS) at  $U = 4$  eV and  $J_H = 0.782$  eV in the paramagnetic states. Extremely flat bands with  $d_{x^2-y^2}$  characters clearly exist near the Fermi level in  $\text{LaFe}_3\text{Si}_2$ . However, such bands in  $\text{LaRu}_3\text{Si}_2$  are not as flat as that in  $\text{LaFe}_3\text{Si}_2$ . By comparing the band structures between the distorted and perfect Kagome lattice of  $\text{LaRu}_3\text{Si}_2$ , we found that the magnitude of distortion of the Kagome lattice have small effects on the flat bands in  $\text{LaRu}_3\text{Si}_2$ . Actually, it is mainly caused by the more extended  $4d$  orbitals that will induce non-vanishing hoppings among distant Kagome lattice sites and result in imperfect destructive interference of hoppings. In  $\text{LaRu}_3\text{Si}_2$ , the flat bands would induce substantial FM fluctuations, as shown in Fig. 3(b).

#### IV. CONCLUSION AND DISCUSSION

To summarize, by taking the Kagome system  $\text{LaX}_3\text{Si}_2$  ( $X=\text{Ru}, \text{Fe}$ ) as an example, we have demonstrated that strong electronic correlations could play important roles in stabilizing a perfect Kagome plane. We show that  $\text{LaRu}_3\text{Si}_2$  is on the verge of becoming a perfect Kagome lattice and it thus exhibits moderate electronic correlation and substantial ferromagnetic fluctuations. Previous study has shown that the electron-phonon couplings

alone are not nearly enough to account for a superconducting  $T_c$  of 7.8 K in  $\text{LaRu}_3\text{Si}_2$ <sup>30</sup>. The electronic correlations and ferromagnetic fluctuations found in our study may play significant roles in enhancing  $T_c$  of  $\text{LaRu}_3\text{Si}_2$ , which is worthy of further study.

As shown in the Fig. S3 in the Supporting Information<sup>41</sup>, the only obvious difference in the simulated powder diffraction pattern of  $\text{LaRu}_3\text{Si}_2$  between the space group  $P6_3/mcm$  and  $P6_3/m$  is an additional reflection at  $(1\ 0\ 1)$  for  $P6_3/m$ . However, its intensity is very weak compared to the main peak such that it is very difficult to be resolved experimentally. Further high-resolution crystal structure refinement with high-quality sample is required to determine whether  $\text{LaRu}_3\text{Si}_2$  crystallizes into the space group  $P6_3/mcm$  or not. Our result thus provides a reference for the crystal structure refinement of  $\text{LaRu}_3\text{Si}_2$ .

#### ACKNOWLEDGMENT

This work was supported by USTC Research Funds of the Double First-Class Initiative (No. YD2340002005). All the calculations presented in this work were performed on TianHe-1A, the National Supercomputer Cen-

ter in Tianjin, China.

- <sup>1</sup> Itiro Syôzi, “Statistics of Kagomé Lattice,” *Progress of Theoretical Physics* **6**, 306–308 (1951).
- <sup>2</sup> A Mielke, “Ferromagnetic ground states for the Hubbard model on line graphs,” *Journal of Physics A: Mathematical and General* **24**, L73 (1991).
- <sup>3</sup> Hal Tasaki, “Ferromagnetism in the Hubbard models with degenerate single-electron ground states,” *Phys. Rev. Lett.* **69**, 1608–1611 (1992).
- <sup>4</sup> Subir Sachdev, “Kagome- and triangular-lattice Heisenberg antiferromagnets: Ordering from quantum fluctuations and quantum-disordered ground states with unconfined bosonic spinons,” *Phys. Rev. B* **45**, 12377–12396 (1992).
- <sup>5</sup> Evelyn Tang, Jia-Wei Mei, and Xiao-Gang Wen, “High-temperature fractional quantum Hall states,” *Phys. Rev. Lett.* **106**, 236802 (2011).
- <sup>6</sup> Yuan Cao, Valla Fatemi, Shiang Fang, Kenji Watanabe, Takashi Taniguchi, Efthimios Kaxiras, and Pablo Jarillo-Herrero, “Unconventional superconductivity in magic-angle graphene superlattices,” *Nature* **556**, 43–50 (2018).
- <sup>7</sup> Leon Balents, Cory R. Dean, Dmitri K. Efetov, and Andrea F. Young, “Superconductivity and strong correlations in moiré flat bands,” *Nature Physics* **16**, 725–733 (2020).
- <sup>8</sup> Hideo Aoki, “Theoretical possibilities for flat band superconductivity,” *Journal of Superconductivity and Novel Magnetism* **33**, 2341–2346 (2020).
- <sup>9</sup> Tero T. Heikkilä and Grigory E. Volovik, “Flat bands as a route to high-temperature superconductivity in graphite,” in *Basic Physics of Functionalized Graphite*, edited by Pablo D. Esquinazi (Springer International Publishing, Cham, 2016) pp. 123–143.
- <sup>10</sup> Kun Jiang, Tao Wu, Jia-Xin Yin, Zhenyu Wang, M Zahid Hasan, Stephen D Wilson, Xianhui Chen, and Jiangping Hu, “Kagome superconductors AV<sub>3</sub>Sb<sub>5</sub> (A=K, Rb, Cs),” *National Science Review* (2022), 10.1093/nsr/nwac199, nwac199.
- <sup>11</sup> Linpeng Nie, Kuanglv Sun, Wanru Ma, Dianwu Song, Lixuan Zheng, Zuowei Liang, Ping Wu, Fanghang Yu, Jian Li, Min Shan, Dan Zhao, Shunjiao Li, Baolei Kang, Zhimian Wu, Yanbing Zhou, Kai Liu, Ziji Xiang, Jianjun Ying, Zhenyu Wang, Tao Wu, and Xianhui Chen, “Charge-density-wave-driven electronic nematicity in a kagome superconductor,” *Nature* **604**, 59–64 (2022).
- <sup>12</sup> Yu-Xiao Jiang, Jia-Xin Yin, M. Michael Denner, Nana Shumiya, Brenden R. Ortiz, Gang Xu, Zurab Guguchia, Junyi He, Md Shafayat Hossain, Xiaoxiong Liu, Jacob Ruff, Linus Kautzsch, Songtian S. Zhang, Guoqing Chang, Ilya Belopolski, Qi Zhang, Tyler A. Cochran, Daniel Multer, Maksim Litskevich, Zi-Jia Cheng, Xian P. Yang, Ziqiang Wang, Ronny Thomale, Titus Neupert, Stephen D. Wilson, and M. Zahid Hasan, “Unconventional chiral charge order in kagome superconductor KV<sub>3</sub>Sb<sub>5</sub>,” *Nature Materials* **20**, 1353–1357 (2021).
- <sup>13</sup> Xiaokun Teng, Lebing Chen, Feng Ye, Elliott Rosenberg, Zhaoyu Liu, Jia-Xin Yin, Yu-Xiao Jiang, Ji Seop Oh, M. Zahid Hasan, Kelly J. Neubauer, Bin Gao, Yaofeng Xie, Makoto Hashimoto, Donghui Lu, Chris Jozwiak, Aaron Bostwick, Eli Rotenberg, Robert J. Birgeneau, Jiun-Haw Chu, Ming Yi, and Pengcheng Dai, “Discovery of charge density wave in a kagome lattice antiferromagnet,” *Nature* **609**, 490–495 (2022).
- <sup>14</sup> Mingu Kang, Linda Ye, Shiang Fang, Jhih-Shih You, Abe Levitan, Minyong Han, Jorge I. Facio, Chris Jozwiak, Aaron Bostwick, Eli Rotenberg, Mun K. Chan, Ross D. McDonald, David Graf, Konstantine Kaznatcheev, Elio Vescovo, David C. Bell, Efthimios Kaxiras, Jeroen van den Brink, Manuel Richter, Madhav Prasad Ghimire, Joseph G. Checkelsky, and Riccardo Comin, “Dirac fermions and flat bands in the ideal kagome metal FeSn,” *Nature Materials* **19**, 163–169 (2020).
- <sup>15</sup> Zhiyong Lin, Chongze Wang, Pengdong Wang, Seho Yi, Lin Li, Qiang Zhang, Yifan Wang, Zhongyi Wang, Hao Huang, Yan Sun, Yaobo Huang, Dawei Shen, Donglai Feng, Zhe Sun, Jun-Hyung Cho, Changgan Zeng, and Zhenyu Zhang, “Dirac fermions in antiferromagnetic FeSn kagome lattices with combined space inversion and time-reversal symmetry,” *Phys. Rev. B* **102**, 155103 (2020).
- <sup>16</sup> Li Huang and Haiyan Lu, “Signatures of hundness in kagome metals,” *Phys. Rev. B* **102**, 125130 (2020).
- <sup>17</sup> Linda Ye, Mingu Kang, Junwei Liu, Felix von Cube, Christina R. Wicker, Takehito Suzuki, Chris Jozwiak, Aaron Bostwick, Eli Rotenberg, David C. Bell, Liang Fu, Riccardo Comin, and Joseph G. Checkelsky, “Massive dirac fermions in a ferromagnetic kagome metal,” *Nature* **555**, 638–642 (2018).
- <sup>18</sup> Zhiyong Lin, Jin-Ho Choi, Qiang Zhang, Wei Qin, Seho Yi, Pengdong Wang, Lin Li, Yifan Wang, Hui Zhang, Zhe Sun, Laiming Wei, Shengbai Zhang, Tengfei Guo, Qingyou Lu, Jun-Hyung Cho, Changgan Zeng, and Zhenyu Zhang, “Flatbands and emergent ferromagnetic ordering in Fe<sub>3</sub>Sn<sub>2</sub> kagome lattices,” *Phys. Rev. Lett.* **121**, 096401 (2018).
- <sup>19</sup> Jia-Xin Yin, Songtian S. Zhang, Hang Li, Kun Jiang, Guoqing Chang, Bingjing Zhang, Biao Lian, Cheng Xiang, Ilya Belopolski, Hao Zheng, Tyler A. Cochran, Su-Yang Xu, Guang Bian, Kai Liu, Tay-Rong Chang, Hsin Lin, Zhong-Yi Lu, Ziqiang Wang, Shuang Jia, Wenhong Wang, and M. Zahid Hasan, “Giant and anisotropic many-body spin-orbit tunability in a strongly correlated kagome magnet,” *Nature* **562**, 91–95 (2018).
- <sup>20</sup> Mingu Kang, Shiang Fang, Linda Ye, Hoi Chun Po, Jonathan Denlinger, Chris Jozwiak, Aaron Bostwick, Eli Rotenberg, Efthimios Kaxiras, Joseph G. Checkelsky, and Riccardo Comin, “Topological flat bands in frustrated kagome lattice CoSn,” *Nature Communications* **11**, 4004 (2020).
- <sup>21</sup> Zhonghao Liu, Man Li, Qi Wang, Guangwei Wang, Chenhaoping Wen, Kun Jiang, Xiangle Lu, Shichao Yan, Yaobo Huang, Dawei Shen, Jia-Xin Yin, Ziqiang Wang, Zhiping Yin, Hechang Lei, and Shancai Wang, “Orbital-selective dirac fermions and extremely flat bands in frustrated kagome-lattice metal CoSn,” *Nature Communications* **11**, 4002 (2020).
- <sup>22</sup> J.-X. Yin, Nana Shumiya, Sougata Mardanya, Qi Wang, Songtian S. Zhang, Hung-Ju Tien, Daniel Multer, Yuxiao Jiang, Guangming Cheng, Nan Yao, Shangfei Wu, Desheng

- Wu, Liangzi Deng, Zhipeng Ye, Rui He, Guoqing Chang, Zhonghao Liu, Kun Jiang, Ziqiang Wang, Titus Neupert, Amit Agarwal, Tay-Rong Chang, Ching-Wu Chu, Hechang Lei, and M. Zahid Hasan, “Fermion–boson many-body interplay in a frustrated kagome paramagnet,” *Nature Communications* **11**, 4003 (2020).
- <sup>23</sup> William R. Meier, Mao-Hua Du, Satoshi Okamoto, Narayan Mohanta, Andrew F. May, Michael A. McGuire, Craig A. Bridges, German D. Samolyuk, and Brian C. Sales, “Flat bands in the CoSn-type compounds,” *Phys. Rev. B* **102**, 075148 (2020).
- <sup>24</sup> Hao Huang, Lixuan Zheng, Zhiyong Lin, Xu Guo, Sheng Wang, Shuai Zhang, Chi Zhang, Zhe Sun, Zhengfei Wang, Hongming Weng, Lin Li, Tao Wu, Xianhui Chen, and Changgan Zeng, “Flat-band-induced anomalous anisotropic charge transport and orbital magnetism in kagome metal CoSn,” *Phys. Rev. Lett.* **128**, 096601 (2022).
- <sup>25</sup> Jia-Xin Yin, Wenlong Ma, Tyler A. Cochran, Xitong Xu, Songtian S. Zhang, Hung-Ju Tien, Nana Shumiya, Guangming Cheng, Kun Jiang, Biao Lian, Zhida Song, Guoqing Chang, Ilya Belopolski, Daniel Multer, Maksim Litskevich, Zi-Jia Cheng, Xian P. Yang, Bianca Swidler, Huibin Zhou, Hsin Lin, Titus Neupert, Ziqiang Wang, Nan Yao, Tay-Rong Chang, Shuang Jia, and M. Zahid Hasan, “Quantum-limit chern topological magnetism in TbMn6Sn6,” *Nature* **583**, 533–536 (2020).
- <sup>26</sup> T. Y. Yang, Q. Wan, J. P. Song, Z. Du, J. Tang, Z. W. Wang, N. C. Plumb, M. Radovic, G. W. Wang, G. Y. Wang, Z. Sun, Jia-Xin Yin, Z. H. Chen, Y. B. Huang, R. Yu, M. Shi, Y. M. Xiong, and N. Xu, “Fermi-level flat band in a kagome magnet,” *Quantum Frontiers* **1**, 14 (2022).
- <sup>27</sup> J.M. Vandenberg and H. Barz, “The crystal structure of a new ternary silicide in the system rare-earth-ruthenium-silicon,” *Materials Research Bulletin* **15**, 1493–1498 (1980).
- <sup>28</sup> Baoxuan Li, Sheng Li, and Hai-Hu Wen, “Chemical doping effect in the LaRu<sub>3</sub>Si<sub>2</sub> superconductor with a kagome lattice,” *Phys. Rev. B* **94**, 094523 (2016).
- <sup>29</sup> Sheng Li, Bin Zeng, Xiangang Wan, Jian Tao, Fei Han, Huan Yang, Zhihe Wang, and Hai-Hu Wen, “Anomalous properties in the normal and superconducting states of LaRu<sub>3</sub>Si<sub>2</sub>,” *Phys. Rev. B* **84**, 214527 (2011).
- <sup>30</sup> C. Mielke, Y. Qin, J.-X. Yin, H. Nakamura, D. Das, K. Guo, R. Khasanov, J. Chang, Z. Q. Wang, S. Jia, S. Nakatsuji, A. Amato, H. Luetkens, G. Xu, M. Z. Hasan, and Z. Guguchia, “Nodeless kagome superconductivity in LaRu<sub>3</sub>Si<sub>2</sub>,” *Phys. Rev. Materials* **5**, 034803 (2021).
- <sup>31</sup> Chunsheng Gong, Shangjie Tian, Zhijun Tu, Qiangwei Yin, Yang Fu, Ruitao Luo, and Hechang Lei, “Superconductivity in kagome metal YRu<sub>3</sub>Si<sub>2</sub> with strong electron correlations,” *Chinese Physics Letters* **39**, 087401 (2022).
- <sup>32</sup> Vladimir I. Anisimov, Jan Zaanen, and Ole K. Andersen, “Band theory and mott insulators: Hubbard U instead of Stoner I,” *Phys. Rev. B* **44**, 943–954 (1991).
- <sup>33</sup> Antoine Georges, Gabriel Kotliar, Werner Krauth, and Marcelo J. Rozenberg, “Dynamical mean-field theory of strongly correlated fermion systems and the limit of infinite dimensions,” *Rev. Mod. Phys.* **68**, 13–125 (1996).
- <sup>34</sup> A. I. Lichtenstein, M. I. Katsnelson, and G. Kotliar, “Finite-temperature magnetism of transition metals: An ab initio dynamical mean-field theory,” *Phys. Rev. Lett.* **87**, 067205 (2001).
- <sup>35</sup> G. Kotliar, S. Y. Savrasov, K. Haule, V. S. Oudovenko, O. Parcollet, and C. A. Marianetti, “Electronic structure calculations with dynamical mean-field theory,” *Rev. Mod. Phys.* **78**, 865–951 (2006).
- <sup>36</sup> Koichi Momma and Fujio Izumi, “VESTA: a three-dimensional visualization system for electronic and structural analysis,” *Journal of Applied Crystallography* **41**, 653–658 (2008).
- <sup>37</sup> G. Kresse and J. Furthmüller, “Efficient iterative schemes for *ab initio* total-energy calculations using a plane-wave basis set,” *Phys. Rev. B* **54**, 11169–11186 (1996).
- <sup>38</sup> P. E. Blöchl, “Projector augmented-wave method,” *Phys. Rev. B* **50**, 17953–17979 (1994).
- <sup>39</sup> John P. Perdew, Kieron Burke, and Matthias Ernzerhof, “Generalized gradient approximation made simple,” *Phys. Rev. Lett.* **77**, 3865–3868 (1996).
- <sup>40</sup> A. I. Liechtenstein, V. I. Anisimov, and J. Zaanen, “Density-functional theory and strong interactions: Orbital ordering in mott-hubbard insulators,” *Phys. Rev. B* **52**, R5467–R5470 (1995).
- <sup>41</sup> See Supporting Information at [url] for: (1) Values of  $U$  and  $J_H$ ; (2) Magnetic configurations; (3) Results of crystal relaxation of LaRu<sub>3</sub>Si<sub>2</sub> by GGA+SOC+U; (4) Simulated XRD pattern of LaRu<sub>3</sub>Si<sub>2</sub> for space group P6<sub>3</sub>/mcm and P6<sub>3</sub>/m.
- <sup>42</sup> Kristjan Haule, Chuck-Hou Yee, and Kyo Kim, “Dynamical mean-field theory within the full-potential methods: Electronic structure of CeIrIn<sub>5</sub>, CeCoIn<sub>5</sub>, and CeRhIn<sub>5</sub>,” *Phys. Rev. B* **81**, 195107 (2010).
- <sup>43</sup> Kristjan Haule and Turan Birol, “Free energy from stationary implementation of the DFT + DMFT functional,” *Phys. Rev. Lett.* **115**, 256402 (2015).
- <sup>44</sup> Peter Blaha, Karlheinz Schwarz, Fabien Tran, Robert Laskowski, Georg K. H. Madsen, and Laurence D. Marks, “WIEN2k: An APW+lo program for calculating the properties of solids,” *The Journal of Chemical Physics* **152**, 074101 (2020).
- <sup>45</sup> Emanuel Gull, Andrew J. Millis, Alexander I. Lichtenstein, Alexey N. Rubtsov, Matthias Troyer, and Philipp Werner, “Continuous-time monte carlo methods for quantum impurity models,” *Rev. Mod. Phys.* **83**, 349–404 (2011).
- <sup>46</sup> Kristjan Haule, “Exact double counting in combining the dynamical mean field theory and the density functional theory,” *Phys. Rev. Lett.* **115**, 196403 (2015).
- <sup>47</sup> Kristjan Haule and Gheorghe L. Pascut, “Forces for structural optimizations in correlated materials within a dft+embedded dmft functional approach,” *Phys. Rev. B* **94**, 195146 (2016).
- <sup>48</sup> See how to use *RCoulombU.py* on EDMFTF’s website .

Supporting Information for “Electronic Correlation Effects on Stabilizing a Perfect Kagome Lattice and Ferromagnetic Fluctuation in  $\text{LaRu}_3\text{Si}_2$ ”

Yilin Wang<sup>1</sup>

<sup>1</sup>*Hefei National Laboratory for Physical Sciences at Microscale,  
University of Science and Technology of China, Hefei, Anhui 230026, China*  
(Dated: March 23, 2023)

---

arXiv:2303.12273v1 [cond-mat.str-el] 22 Mar 2023

TABLE S1. Values of Hubbard  $U$  and Hund's coupling  $J_H$  calculated by the code *R\_Coulomb.py* in DFT+EDMFTF package. These values are used for both DFT+ $U$  and LDA+DMFT calculations.

$U$ (eV)	1.1	1.5	2.0	3.0	4.0	4.5	5.0	5.5	6.0
$J_H$ (eV)	0.389	0.476	0.563	0.692	0.782	0.817	0.848	0.874	0.897

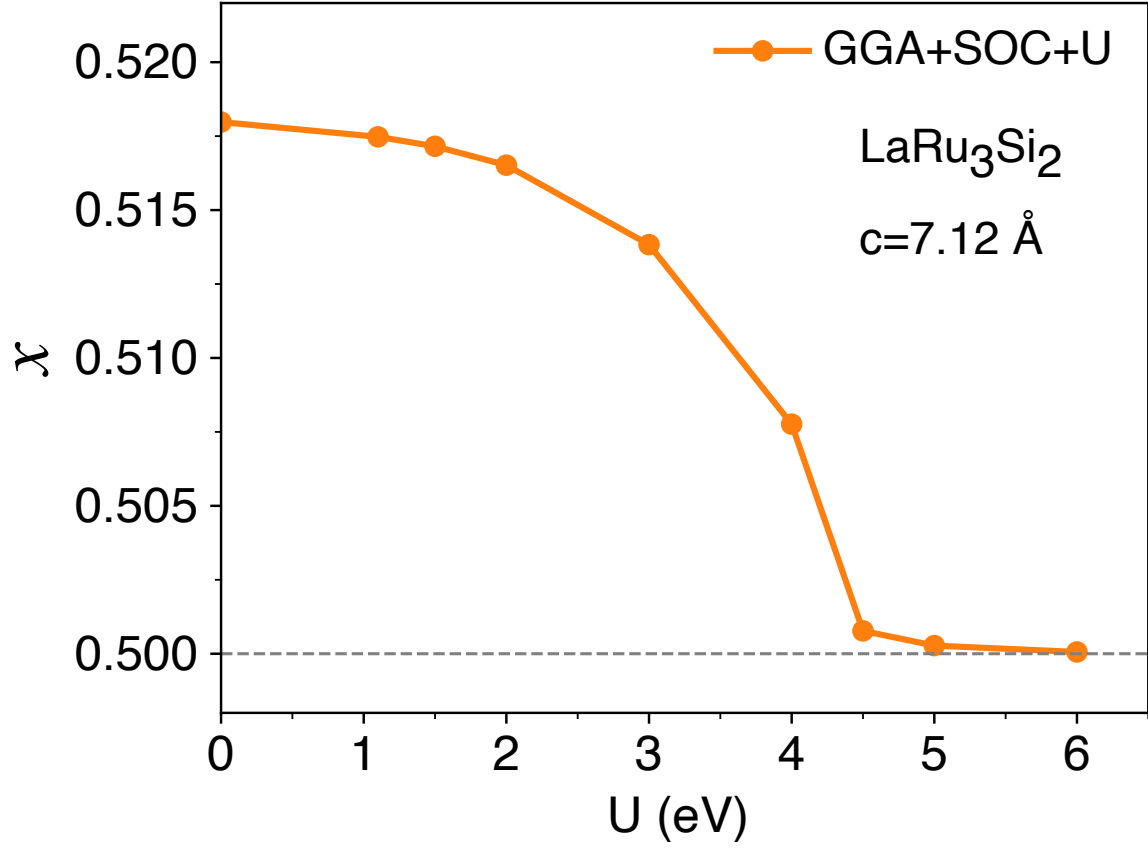


FIG. S1. Fractional coordinates  $x$  of Ru sites as function of Hubbard  $U$ , relaxed by GGA+ $U$  with spin-orbital coupling.

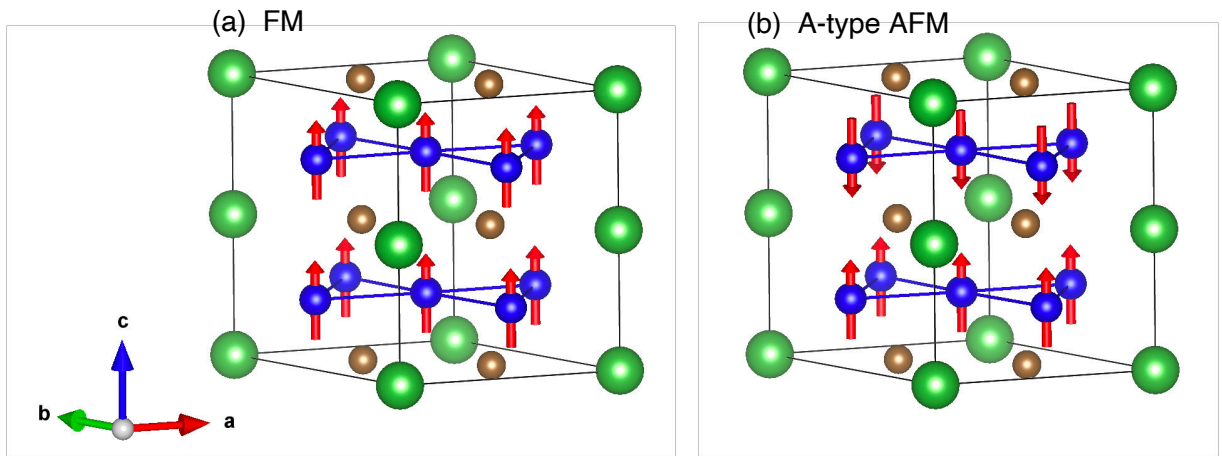


FIG. S2. Magnetic configurations considered in the GGA+ $U$  calculations.



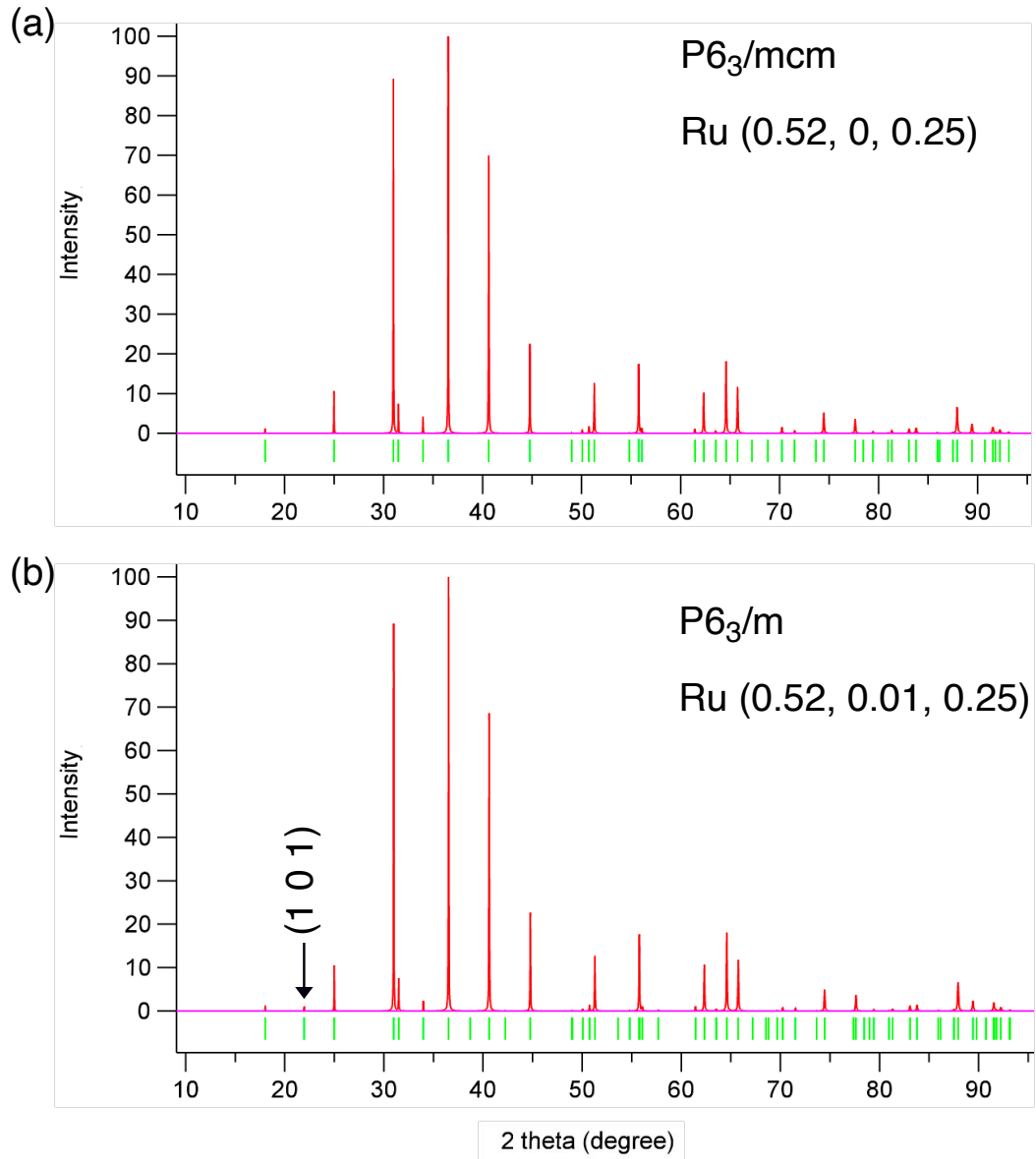


FIG. S3. Simulated XRD pattern of the possible distorted Kagome structure of  $\text{LaRu}_3\text{Si}_2$ . (a) For space group  $P6_3/mcm$  with Ru at (0.52, 0, 0.25). (b) For space group  $P6_3/m$  with Ru at (0.52, 0.01, 0.25). Lattice parameters are  $a = 5.676\text{\AA}$  and  $c = 7.12\text{\AA}$ . Their only difference is that there is an additional weak peak at (1 0 1) for  $P6_3/m$ .